Journal of South American Earth Sciences 103 (2020) 102715

Contents lists available at ScienceDirect

Journal of South American Earth Sciences

journal homepage: www.elsevier.com/locate/jsames

Bedrock and detrital zircon thermochronology to unravel exhumation histories of accreted tectonic blocks: An example from the Western Colombian Andes

S. Zapata [a,b,*], A. Patiño [c], A. Cardona [d,e], M. Parra [c], V. Valencia [f], P. Reiners [g], F. Oboh-Ikuenobe [b], F. Genezini [h]

[a] Smithsonian Tropical Research Institute, Balboa, Ancon, Panama
[b] Department of Geosciences and Geological and Petroleum Engineering, Missouri University of Science and Technology, USA
[c] Institute of Energy and Environment, University of So Paulo, São Paulo, Brazil
[d] Departamento de Procesos y Energía, Facultad de Minas, Universidad Nacional de Colombia, Medellín, Colombia
[e] Grupo de Investigación en Geología y Geofísica (EGEO), Universidad Nacional de Colombia, Colombia
[f] School of the Environment, Washington State University, USA
[g] Department of Geosciences, University of Arizona, USA
[h] Instituto de Pesquisas Energéticas e Nucleares, São Paulo, Brazil

A B S T R A C T

The Northern Andes are the result of multiple tectonic phases, which include extensional and compressional volcanic arcs, strike-slip fragmentation, and accretion of exotic terranes. The alternations of these tectonic settings have overprinted and fragmented the geological record, which has hindered precise paleogeographic and tectonic reconstructions. In the western segment of the Colombian Andes, the oceanic-cored Western Cordillera (WC) and the continental Central Cordillera (CC) are separated by the Romeral Fault Zone (RFZ). This segment of the Andes preserves the record of Cretaceous back-arc extension, the onset of compression, and the accretion of the Caribbean plateau during the Late Cretaceous-Paleocene. To refine the tectonic evolution of the Western Colombian Andes, this study documents new detrital zircon fission-track (ZFT) data from the Meso-Cenozoic sedimentary cover in the CC, the RFZ, and the WC; new ZFT and zircon helium (ZHe) bedrock data from the CC and the RFZ; and new U–Pb detrital data from the Miocene sedimentary cover of the RFZ. Within the RFZ, we obtained bedrock ZFT ages of 239.0 ± 11.0 Ma and 111.1 ± 4.3 Ma, and detrital ZFT data from the Abejorral Formation are interpreted as the result of post-magmatic cooling and Cretaceous rifting. Late Cretaceous to Eocene ZFT and ZHe ages (~61–50 Ma) in the CC and detrital ZFT data in the WC record exhumation and deformation of the CC during and after the collision of the Caribbean plateau with the continental margin. Finally, detrital U–Pb and ZFT data from the Amagá Formation record the formation of a Miocene intermountain basin. This study reconstructs the basin geometries and the deformation patterns before, during, and after the collision of the Caribbean plateau with the South American margin. We highlight that in accretionary orogens, in which prolonged deformation and erosion have removed the sedimentary cover, the quantification of differential basement exhumation is key to reconstruct thick-skin deformation and to define major tectonic boundaries.

1. .Introduction

Alternations among extensional and compressional tectonic regimes controlled the Mesozoic and Cenozoic sedimentation and deformation patterns of the Northern Andes. These tectonic cycles have resulted from changes in the subduction angle, variations of the rates and direction of convergence, and the accretion of exotic terranes to the South American continental margin (Cardona et al., 2012, 2011; León et al., 2018; Montes et al., 2019; Spikings et al., 2015; Zapata et al., 2019a). The Romeral Fault Zone (RFZ) defines the suture between the basement of the Central and Western Cordilleras (CC and WC). In this segment of the Northern Andes, the alternations between tectonic regimes and associated strike-slip deformation have complicated the precise paleogeographic and tectonic reconstructions between the Cretaceous and Eocene (Montes et al., 2019; Spikings et al., 2015; Zapata et al., 2019a). Moreover, the absence of these stratigraphic markers makes difficult the correlation with adjacent tectonic blocks and the reconstruction of Late Cretaceous to Paleogene deformational phases (e.g. Restrepo and Toussaint, 1988; Villagómez et al., 2011a; Zapata et al., 2019a).

In the Northern Andes, major tectonic boundaries are used to separate tectonic blocks with dissimilar chronostratigraphic records, which are interpreted as formed at different paleogeographic positions and in contrasting tectonic settings (Montes et al., 2019; Restrepo and Toussaint, 2020, 1991; 1988; Spikings et al., 2014). However, the lack of

* Corresponding author. Smithsonian Tropical Research Institute, Balboa, Ancon, Panama.
E-mail addresses: szapatah@gmail.com, ZapataS@Si.edu (S. Zapata).

https://doi.org/10.1016/j.jsames.2020.102715
Received 13 April 2020; Received in revised form 6 June 2020; Accepted 22 June 2020
Available online 28 June 2020

constraints in the amount and time of relative lateral and vertical displacements between adjacent tectonic blocks difficult the accurate definition of these major tectonic boundaries (Zapata et al., 2019a), which may lead to interpret different structural levels of a single crustal domain juxtaposed along faults as terrane boundaries (e.g. Broussolle et al., 2019; Guy et al., 2020). Low-temperature thermochronology can be a powerful tool to constraint relative exhumation differences between adjacent basement-core tectonic blocks (e.g. Löbens et al., 2013; Pearson et al., 2013; Sobel et al., 2006b).

The comparison between the detrital record and potential source areas (source to sink approach) has the potential to provide key information for understanding former basin geometries and syn-depositional tectonic settings (Horton et al., 2010; León et al., 2019; Malusà and Garzanti, 2019; Mora et al., 2010). In the Northern Andes, the along-strike similarities of rock units and U–Pb zircon populations have reduced the resolution of several provenance techniques to identify along-strike movements. However, since exhumation histories are different along the strike of the Northern Andes (e.g. Spikings et al., 2014; Villagómez and Spikings, 2013), detrital thermochronology may be an alternative to constraint along-strike displacements. Moreover, the integration of detrital and bedrock thermochronology allows the identification of cooling events from eroded source areas, reconstruction of the long-term basin and bedrock thermal histories, and unravel the relationship between sediment accumulation and basement exhumation (Lag-time) (e.g. Bernet et al., 2006; Malusà and Fitzgerald, 2019; Malusà and Garzanti, 2019; Sobel et al., 2006a).

we obtained zircon (U–Th)/He (ZHe) and zircon fission-track (ZFT) data from detrital and bedrock samples to reconstruct deformation and sedimentation patterns across major tectonic boundaries and constraint relative vertical fault displacements. Our study area comprises an ~80 km long ~ E-W segment of the Western Colombian Andes between 5°40′N and 5°50′N (Fig. 1), which includes the continental basement of the CC, the units embedded in the RFZ, and the volcanic basement of the WC. The sampled units include a pre-Mesozoic metamorphic and igneous basement, the Cretaceous to Cenozoic volcano-sedimentary cover in the CC and the RFZ, and the Cretaceous sedimentary cover in the WC.

2. Tectonic evolution of the Western Colombian Andes

The Jurassic to Miocene tectonic evolution of the Northern Andes comprises a period of extensional tectonics and strike-slip fragmentation between 150 Ma and 90 Ma (Montes et al., 2019; Zapata et al., 2019a), compression between 90 Ma and 70 Ma, oblique accretion of the Caribbean oceanic crust between 70 Ma and 60 Ma (Bayona et al., 2012; Cardona et al., 2012; Montes et al., 2019; Spikings et al., 2015; Zapata et al., 2019a), and Neogene compression due to both the accretion of the Panama-Chocó terrane and an increase in the tectonic coupling between the Nazca and the South American plates (León et al., 2018; Montes et al., 2019, 2015; Parra et al., 2009).

The Western Colombian Andes comprises the CC and WC, and the Cauca Valley in between them. Within this valley is the RFZ, which is a Late Cretaceous tectonic suture between the continental rocks in the CC and the exotic oceanic crust in the WC (Figs. 1 and 2)(Maya and Gonzalez, 1995; Vinasco and Cordani, 2012). The basement of the CC is characterized by the presence of low to medium-grade metamorphic rocks grouped into the Cajamarca Complex, which is intruded by Permo-Triassic and Meso-Cenozoic granitoids (Figs. 1 and 2) (Leal-Mejia, 2011; Leal-Mejía et al., 2019; Spikings et al., 2014; Vinasco et al., 2006). This metamorphic basement is unconformably overlain by the clastic Cretaceous sediments (130–100 Ma) of the Abejorral Formation (Fig. 2). This unit is characterized by transgressive clastic volcano-sedimentary successions accumulated in transitional and shallow marine depositional systems (Rodríguez and Rojas, 1985; Zapata et al., 2019a). The Abejorral Formation has been interpreted as being formed in a back-arc basin during the Early Cretaceous (León et al., 2019; Zapata et al., 2019a).

Located in the eastern segment of the RFZ is the Quebradagrande Complex; this unit is a fault-bounded volcano-sedimentary succession formed between 95 and 80 Ma (Jaramillo et al., 2017; Zapata et al., 2019a). Between 97 and 58 Ma, arc-related magmatism of the Antioquia Batholith and the Aguadas Porphyry intruded the continental basement and the Cretaceous sedimentary cover in the CC (Duque-Trujillo et al., 2019 and references therein). Late Cretaceous magmatic record hosted in the basement of the CC and the magmatism of the Quebradagrande Complex have been interpreted as parts of a continental volcanic arc, formed during contraction (97–58 Ma), after the closure of the former back-arc basin (Jaramillo et al., 2017; Zapata et al., 2019a).

The Arquía Complex is located in the western segment of the RFZ and it is composed of Mesozoic low to medium-grade schists and amphibolites, and high-pressure metamorphic rocks. High-pressure rocks have been interpreted as parts of a subduction complex formed at ~129 Ma and exhumed at ~115 Ma (Fig. 2) (Avellaneda-Jiménez et al., 2019; Bustamante et al., 2011; García-Ramírez et al., 2017; Maya and Gonzalez, 1995). Deformational fabric from Cretaceous and Permo-Triassic rocks located within the RFZ have Ar–Ar isotopic ages between 120 Ma and 65 Ma. These ages have been attributed to fault activity within the RFZ (Vinasco and Cordani, 2012).

The San Jerónimo Fault separates the CC and the RFZ (Figs. 1 and 2). Since the record of the Quebradagrande Complex within the RFZ has been interpreted as formed in intra-oceanic settings distant from the continental margin, the San Jerónimo Fault has been proposed as a regional terrane boundary, which separates the CC and the rocks of the Quebradagrande Complex (Fig. 1) (Maya and Gonzalez, 1995; Spikings et al., 2015; Villagómez et al., 2011a). However, more recent studies have proposed that the Quebradagrande Complex is a fringing arc formed in the continental margin (Zapata et al., 2019a). The Cauca-Almaguer Fault is a major terrane boundary that separates the RFZ from the WC (Restrepo and Toussaint, 2020, 1991; 1988; Spikings et al., 2014). Previous studies of this fault system have focus on understanding the strike-slip movements of this fault (Montes et al., 2019; Vinasco and Cordani, 2012); however, vertical displacement along this fault has been poorly studied.

The basement of the WC is composed of mafic volcanic rocks that were part of the Caribbean oceanic plateau (Hincapié-Gómez et al., 2018; Kerr et al., 1997; Vallejo et al., 2006). Between ~100 Ma and 80 Ma, west-dipping subduction beneath the eastern edge of the Caribbean plate formed an island arc on top of the Caribbean basement. The record of this volcanic arc includes several granitic intrusives and volcanic lavas of the Barroso Formation (Fig. 2) (Cetina et al., 2019; Rodriguez and Zapata, 2013; Spikings et al., 2015; Zapata et al., 2017). During the Late Cretaceous-Paleocene, the eastern Caribbean plateau collided with the South American continental margin. As a result, a portion of the plateau and its associate island arc were accreted to South America (region between the Cauca-Almaguer Fault and the Uramita Fault, Fig. 1) (Kerr and Tarney, 2005; Montes et al., 2019; Pardo-Trujillo et al., 2020; Spikings et al., 2014; Zapata et al., 2019a). The Penderisco Formation is a volcano-clastic succession unconformably deposited on top of the accreted plateau and is divided into the siliciclastic Urrao and calcareous Nutibara members (González, 2001). The Urrao Member was deposited between the Late Campanian to Paleocene (Pardo-Trujillo et al., 2020) and its provenance exhibits sources from the CC (Pardo--Trujillo et al., 2020). This unit has been interpreted as the sedimentary record before and coeval with the collision between the Caribbean plateau and the continental margin (Pardo-Trujillo et al., 2020). In the WC has not been found a sedimentary record with depositional ages between ~50 and 30 Ma (León et al., 2018; Pardo-Trujillo et al., 2020).

The Amagá Formation is an epiclastic sedimentary succession deposited unconformably on top of the rocks within the RFZ in a fluvial depositional system during the middle Oligocene-Late Miocene (Fig. 2) (Van der Hammen, 1960). This unit has been divided into three members, the lower member comprises successions of interbed polymictic

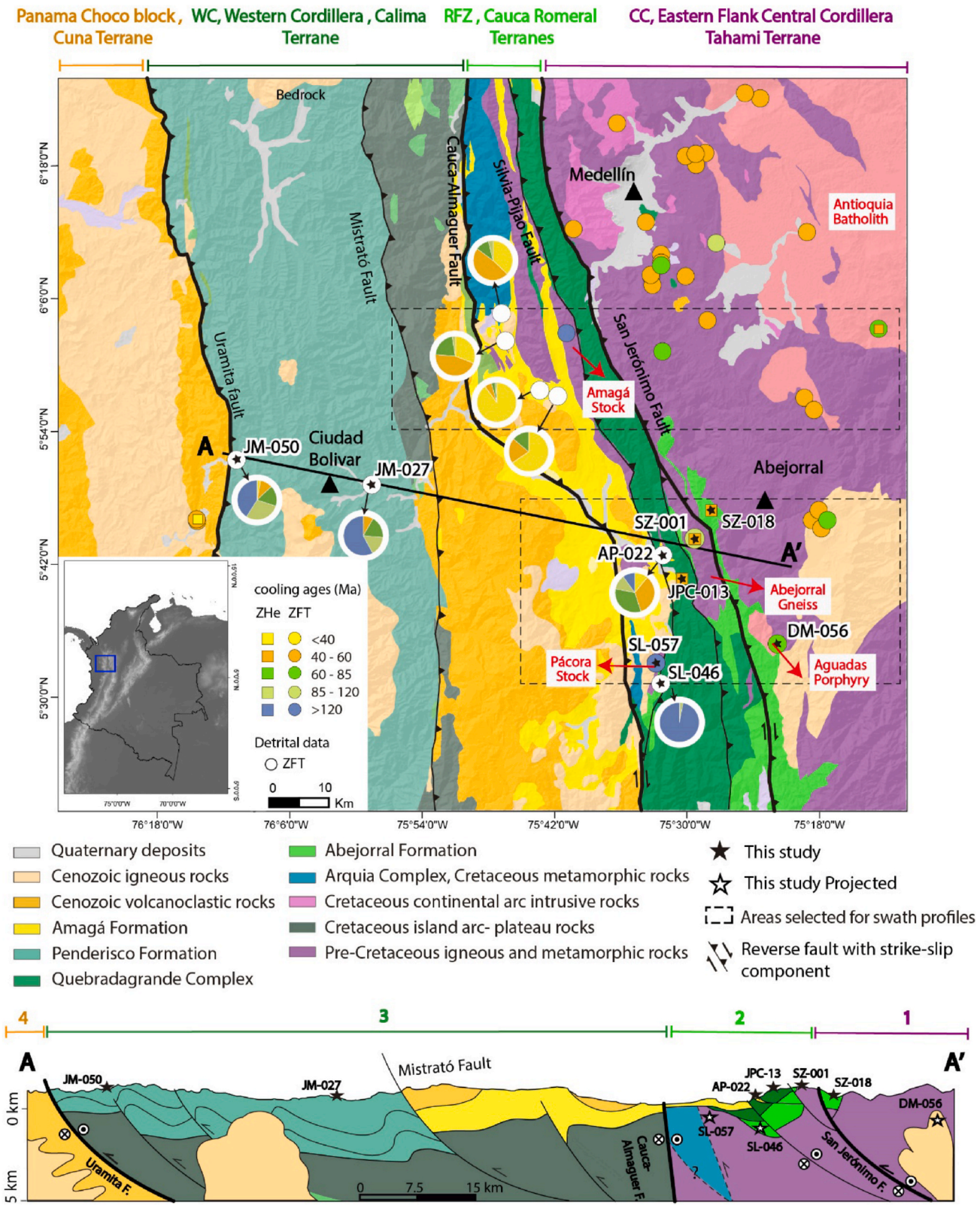

Fig. 1. Geological map and cross-section of the study area, modified from Gómez et al. (2015). Dashed squares represent the transects presented in Fig. 5. Squares and circles indicate available ZHe and ZFT thermochronological data (Montes, 2007; Saenz, 2003; Villagómez et al., 2011b), black stars represent the data presented in this contribution, pie charts represent thermochronological detrital data, and color code denotes sample thermochronological age, the used data is presented in Table S2. Colored captions in the upper segment of the map and the cross-section denote major tectonic blocks and their equivalent terrane definition according to Restrepo and Toussaint (2020). Black thick lines denote the structures interpreted as major tectonic boundaries. Vertical exaggeration in cross-section is 1:3. (For interpretation of the references to color in this figure legend, the reader is referred to the Web version of this article.)

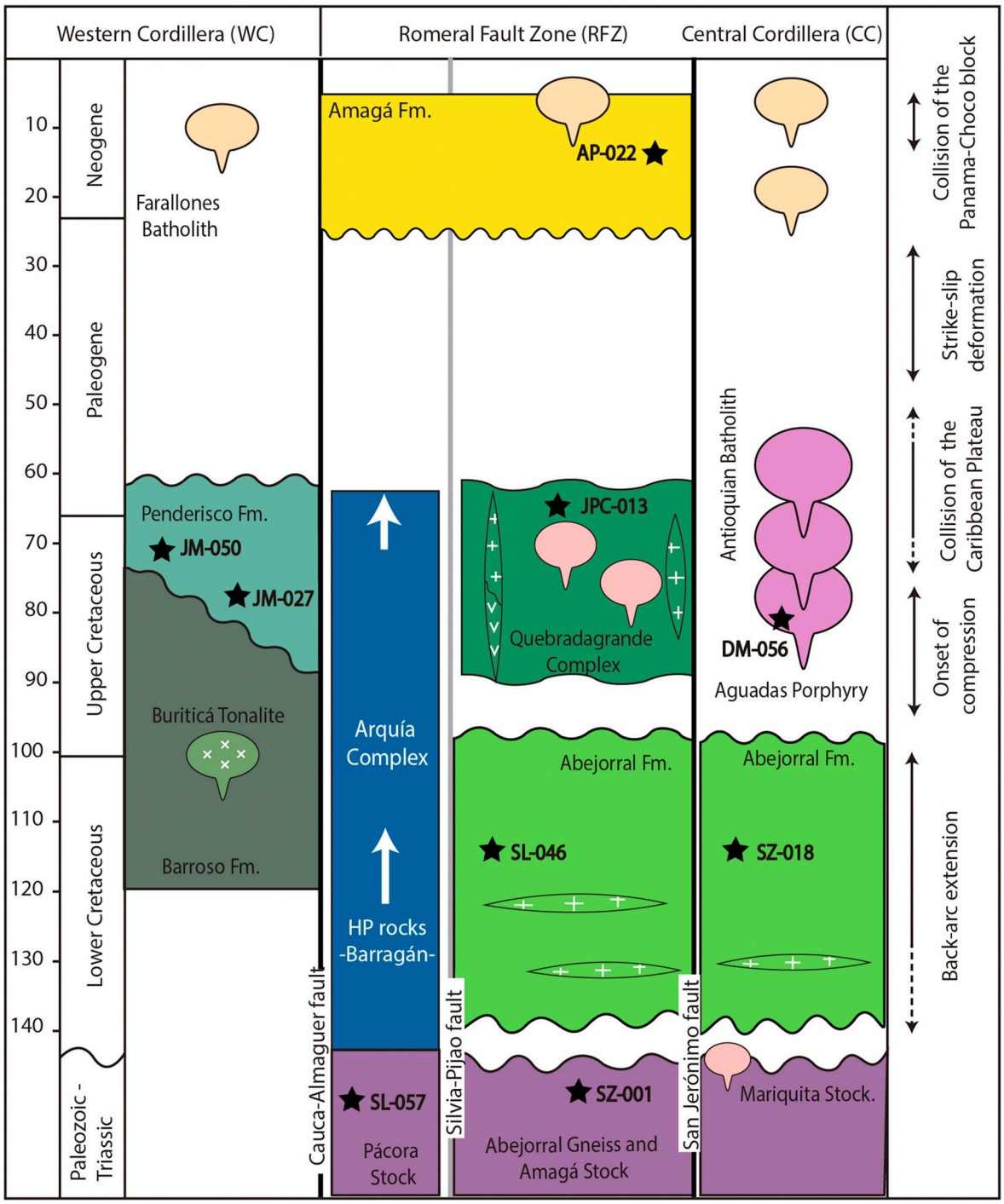

Fig. 2. Chronostratigraphic chart of the Cretaceous to Cenozoic units in the study area. The right panel contains interpreted tectonic settings (Spikings et al., 2015; Zapata et al., 2019a). Fm. = Formation. Black stars denote the samples presented in this contribution.

conglomerates, sandstones with cross-stratification, mudstones, and minor coal beds; the middle member is characterized by an increase in the thickness and abundance of coal beds; and the upper member is composed mostly of sandstone and claystone (González, 2001). This unit has been interpreted as being accumulated in a fluvial system within a pull-apart basin between the CC and WC (Sierra Lopera et al., 2012). Furthermore, several studies have interpreted the sedimentary record of the Amagá Formation as syn-orogenic strata that were coeval with the late phases of the Andean orogeny (Lara et al., 2018a; Silva-Tamayo et al., 2008).

3. Analytical approach, ZFT and ZHe thermochronology of the Northern Andes

Thermochronology is based on the quantification of the products of radioactive decay that are accumulated after the closure of a radioisotope system (Dodson, 1973; Harrison, 2005; Reiners and Zeitler, 2005). For each system, the closure temperature approximately marks the condition at which such products can be retained within the mineral structure (Dodson, 1973; Gallagher et al., 2002; Guenthner et al., 2013). Therefore, thermochronology can quantify the time that has passed since a rock body cooled below the closure temperature of the isotopic

system (Reiners and Brandon, 2006; Reiners and Zeitler, 2005).

In upper crustal levels, rock cooling can be related to the relative movement of rock bodies from deeper crustal levels towards the surface (exhumation), the emplacement of magmatic bodies, and regional changes in the thermal state of the crust (Malusà and Fitzgerald, 2019; Murray et al., 2018; Reiners and Zeitler, 2005). Therefore, thermochronology has the potential to unravel multiple tectonic events, such as footwall exhumation during normal faulting, hanging wall exhumation due to intense erosion promoted by inverse faulting and topographic growth, and post-magmatic cooling. Past cooling events can be preserved in the detrital record of adjacent sedimentary basins as long as the closure temperatures of the studied isotopic system were not surpassed (Malusà and Garzanti, 2019).

The pre-Cenozoic basement of the Northern Andes yield ZFT and ZHe ages between ~250 and 10 Ma (e.g. Amaya and Centenaro, 1997; Spikings et al., 2000, 2005; Villagómez and Spikings, 2013). The northern segment of the CC (>5 °N) is characterized by ZFT ages between ~50 and 70 Ma, while its southernmost segment (~1 °N) ZFT ages are significantly older ages (106 and 112 Ma) (Villagómez and Spikings, 2013). Further south, in The Cordillera Real of Ecuador ZFT ages, is between 35 and 70 Ma (Spikings et al., 2000, 2005). The northern segment of the WC has two ZFT ages of ~41 and 46 Ma (Montes, 2007; Saenz, 2003; Villagómez and Spikings, 2013). Inland, the Eastern Cordillera of Colombia is characterized by the presence of Oligocene and Miocene ZFT ages and the absence of Late Cretaceous to Paleocene exhumation (e.g. Mora et al., 2019). Farther north in the Santander massif ZFT ages between 40 and 65 Ma have not been reported, in this region, most ZFT ages are Lower Cretaceous and Jurassic (Amaya et al., 2017; van der Lelij et al., 2016).

ZHe ages from the basement of the Northern Andes are more scarce. Available data include ages between 60 and 40 Ma in the northern segments of the Central and Eastern Cordilleras of Colombia (Fig. 5A), one Oligocene basement age from the WC of Colombia, and one Miocene age from the southern segment of the CC of Colombia (Caballero et al., 2013; Noriega-Londoño et al., 2020; Villagómez and Spikings, 2013). Despite the lack of spatial and temporal resolution of the available ZFT and ZHe data in several segments of Northern Andes (e.g. CC between ~2 and 5 °S), some provinces show distinctive ZFT and ZHe age populations that have the potential to refine the links between sedimentary basins and source areas along the Northern Andes.

Herein, we compare the thermal evolution of the basement blocks and the adjacent sedimentary successions to reconstruct Cretaceous to Cenozoic extensional and compressional settings in the Western Colombian Andes. ZFT and ZHe dating was used to interpret long-term thermal histories as a response to different tectonic settings. We sampled basement and sedimentary rocks located in different tectonic blocks along an ~ E-W segment between the CC and WC. This sampling design allowed us to compare the Mesozoic and Cenozoic thermal evolution of the basement and the associated basins in different structural positions. The zircons analyzed in this study are aliquots from samples with published U–Pb zircon ages (Cardona et al., 2019; Pardo-Trujillo et al., 2020; Zapata et al., 2019a).

4. Methods

4.1. Zircon fission-track (ZFT) methods and procedures

The ZFT method is based on the quantification 'of damage to the crystal lattice (tracks) that results from the spontaneous fission of ^{238}U. Estimates of the closure temperature for the ZFT system depend on cooling rates, these temperatures vary between ~200 °C and 240 °C for field-based studies (Bernet, 2009; Brandon et al., 1998; Zaun and Wagner, 1985) to up to 350 °C for laboratory-based studies (Tagami et al., 1998; Yamada et al., 2007), the differences being ascribed to the effect of radiation damage (Bernet, 2009).

Sample preparation was performed at the Low-Temperature Thermochronometry (LabTer), at the Institute of Energy and Environment (IEE) at the University of São Paulo (USP). From each sample, three zircon aliquots were mounted in PTFE sheets following the multimount technique (Naeser and Faul, 1969), polished, and then etched using in a eutectic solution of KOH: NaOH at a temperature of 228 °C (Gleadow et al., 1976) for times varying between 12 and 20 h.

After etching, the aliquots and CN-1 dosimeter glasses were covered with U-free mica sheets and irradiated with thermal neutrons at the IEA-R1 research reactor, IPEN-University of São Paulo, using an irradiation fluency of 5E14 n/cm^2. Subsequently, mica detectors were etched for 40 min at 21 °C with 40% HF to reveal induced tracks. All samples were analyzed at the LabTer at the IEE-USP using an Olympus BX51 optical microscope with a magnification of 1600X and the FT-Stage system (Dumitru, 1993). Age calculations were made using a zeta factor of 135.1 ± 3.0 (Patiño, A.).

A minimum of 20 grains were analyzed to calculate each bedrock age and around 100 grains for detrital samples. The ZFT age distributions were tested using the chi-squared statistical to evaluate if they represent a unique population (Galbraith and Laslett, 1993; Green, 1981). When P (χ^2) was higher than 5%, cooling ages are considered to be part of the same age population. For detrital samples, we extracted the main age population peaks using the binomial peak fitting method (Galbraith and Laslett, 1993) and the BINOMFIT software (Brandon, 1996). ZFT data is presented in Table 1 and individual grain counts in Table S3.

4.2. Zircon U–Th/He (ZHe) method and procedures

ZHe thermochronology exploits the thermally activated accumulation of He in the mineral lattice of zircons resulting from the alpha decay of ^{238}U, ^{235}U, ^{232}Th, and ^{147}Sm to ^{206}Pb, ^{207}Pb, ^{208}Pb, and ^{143}Nd, respectively. In zircon, helium can be retained within the mineral lattice at temperatures between 140 °C and 220 °C, which is called the zircon partial retention zone (ZPRZ), depending on the crystal's radiation damage (Guenthner et al., 2013). Radiation damage effects can be spotted by identifying a correlation between single grain ZHe ages and effective uranium content (eU = [U]+0.235[Th]). To assess intra-sample dispersion, we consider ages to be reproducible when the 1σ S.D. is <20% of the mean age (Flowers, 2009; Flowers and Kelley, 2011).

Measurements of parent and daughter nuclides in zircon grains were performed at Arizona University following the protocol presented in Reiners (2005). Tetragonal crystals with prism widths of at least 70 μm were hand-picked, photographed, and packed in individual Nb foils. Each foil packet was directly heated using a 10 nm focused beam of 1064-nm Nd-YAG laser for 15 min extraction intervals. U and Th nuclides in degassed zircons were measured by isotope dilution and solution ICP-MS. Detailed lab procedures are described in Zapata et al. (2014).

4.3. U–Pb zircon geochronology

We performed zircon U–Pb dating on zircon grains from one sample for single grain provenance from the Amagá Formation The Laser Ablation Inductively Coupled Plasma Mass Spectrometry (LA-ICP-MS) U–Pb analyses were conducted at Washington State University using a New Wave Nd:YAG UV 213-nm laser coupled to a Thermo Finnigan Element 2 single collector, double-focusing, magnetic sector ICP-MS. Operating procedures and parameters were similar to those of Chang et al. (2006). Laser spot sizes and repetition rates were 30–20 μm and 10 Hz, respectively. U and Th concentrations were monitored by comparing to NIST 610 trace element glass. Only the cores of the grains were analyzed to avoid complex zircon histories (Gehrels et al., 2006). We obtained 103 ages, from these we rejected data with concordance percentages below 90 and above 110% (n = 14). The concordant data were used to obtain the main age populations employing the software Isoplot R (Vermeesch, 2018). Analytical results are presented in Table S4.

Table 1
Bedrock zircon fission-track data.

Sample	Tectonic block	Unit	Unit/U–Pb crystallization age (Ma)	n	Ns	Rhos (cm $^{-2}$)	Ni	Rhoi (cm $^{-2}$)	Nd	U (ppm)	P(□^{2}) (%)	Dispersion (%)	Central age (Ma)	1σ (Ma)
SL-057	CC	Pácora stock	(260.5 ± 4.7Ma)	23	1723	1.86E+07	1076	1.16E+07	4121	160.7	20	10	239	11
SZ-001	CC	Abejorral Gneiss	(274.0 ± 9.6Ma)	27	1757	7.61E+06	2452	1.06E+07	4121	160.5	9	11	111.1	4.3
DM-056	CC	Aguadas Porphyry	(97.43 ± 0.75Ma)	20	796	2.58E+06	1933	6.27E+06	4116	85.2	29.5	7.4	64.6	2.9

[1] Published U–Pb ages for each sample (Cardona et al., 2019; Vinasco et al., 2006; Zapata et al., 2019a), sample coordinates are presented in Table S1 ζ = 135.1 ± 3.0 (Patiño, A.).

5. Results

We obtained ZFT and ZHe data from three samples from the metamorphic and igneous basement of the CC and the RFZ, including ZHe and ZFT data from the Permo-Triassic Abejorral gneiss (SZ-001), ZFT data from the Permo-Triassic Pácora stock (SL-057), and ZFT data from the Late Cretaceous Aguadas Porphyry (DM-056). We obtained ZHe data from one sample from the Abejorral Formation from the CC and one sample of the Quebradagrande Complex from the RFZ (SZ-018 and JPC-013, respectively). Finally, detrital ZFT data were derived from two samples of the Penderisco Formation from the WC, one sample of Abejorral Formation from the RFZ, and one sample of the Amagá Formation from the RFZ. U–Pb geochronology was performed on zircon grains from the Late Oligocene-Middle Miocene Amagá Formation in the RFZ (Fig. 1, Table S1).

5.1. Thermochronology

5.1.1. Permo-Triassic rocks (RFZ)

We performed ZFT dating on 23 zircon grains from a sample from the Pácora Stock (SL057), which is located in the western limit of the RFZ (Fig. 1). This sample has individual ages between 162.3 Ma and 308.7 Ma with U content between 83.6 ppm and 325.2 ppm. The age distribution has a central age of 239.0 ± 11.0 Ma, with a P (χ^2) value of 0.20 (Table 1; Fig. 3A). We performed ZFT dating on 27 zircon grains from one sample from the Abejorral Gneiss (SZ-001), which is located in the eastern segment of the RFZ (Fig. 1). This sample exhibits individual ZFT ages between 75.9 Ma and 143.3 Ma, with U content between 78.0 and 307.2 ppm. The age distribution has a central age of 111.1 ± 4.3, with a P (χ^2) value of 0.09 (Table 1; Fig. 3A). From sample SZ-001, we obtained four reproducible ZHe single grain ages with a mean age of ~50 Ma, the ESR values vary between 33.9 μm and 40.7 μm and eU values are between 126.1 ppm and 517.7 ppm (Table 3; Fig. 3D).

5.1.2. Aguadas Porphyry (CC)

We performed ZFT dating on 20 single grains from a sample from the Aguadas Porphyry (DM056), which is located east of the San Jerónimo Fault in the western flank of the CC (Fig. 1). This sample has single grain ZFT ages between 46.8 Ma and 85.2 Ma, with U content between 51.7 ppm and 139.4 ppm. The age distribution has a central age of 64.6 ± 2.9 Ma, with a P(χ^2) value of 0.30 (Table 1; Fig. 3A).

5.1.3. Abejorral Formation (CC and RFZ)

We performed detrital ZFT dating on 99 grains from a sandstone sample from the Abejorral Formation (SL046), which was collected in the western segment of the RFZ (Fig. 1). This sample has single grain ZFT ages between 83.6 Ma and 961.9 Ma, with uranium content between 26.4 ppm and 342.1 ppm, and data dispersion of 40%. This sample preserves detrital ZFT signatures with age peaks at 128.2 Ma, 268.1 Ma, and 511.6 Ma (Table 2; Fig. 3B and C). ZHe dating was performed on an andesitic lava sample (SZ-018) from the Upper Abejorral Formation, collected in the western flank of the CC, east of the San Jerónimo fault (Fig. 1). We obtained four reproducible ZHe single grain ages, with a mean age of ~50 Ma. ESR values are between 39.4 μm and 101.9 μm and eU values are between 61.7 ppm and 140.6 ppm (Table 3, Fig. 3D).

5.1.4. Quebradagrande Complex (RFZ)

We performed ZHe dating on four zircon grains from andesitic lava from the Quebradagrande Complex (JPC013) located within the RFZ. ZHe single grain ages are reproducible and have a mean age of ~57 Ma, with ESR values between 44.5 μm and 63.3 μm, and eU values between 216.7 and 485.6 ppm. Despite age reproducibility, single grain ZHe ages exhibit a positive correlation with the eU values (Table 3; Fig. 3D).

5.1.5. Penderisco Formation (WC)

We dated two sandstone samples from the Penderisco Formation

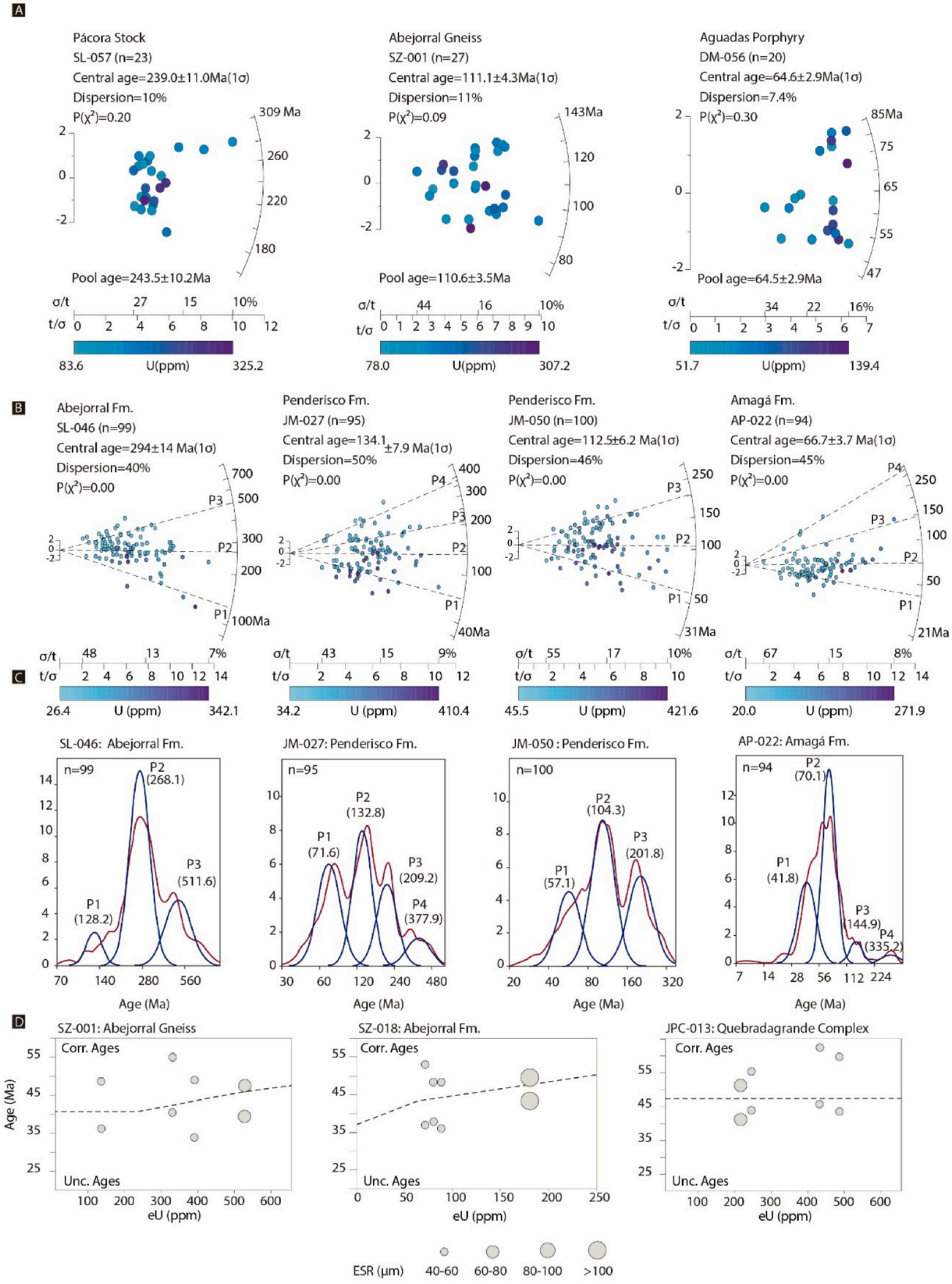

Fig. 3. Results of the ZFT and ZHe thermochronology. A) Bedrock ZFT ages, color code denotes single grain uranium content. B) ZFT detrital ages, color code denotes single grain uranium content and dash lines represent each age population. C) ZFT detrital ages, red line denotes the probability distribution and the blue lines the modeled age peaks (Binomfit). D) Age vs eU plots of the single grain ZHe ages, dot size indicates the equivalent spherical radius (ESR). Dash lines, separate corrected and uncorrected ages. Radial plots were made with RadialPlotter program of Vermeesch (2009). (For interpretation of the references to color in this figure legend, the reader is referred to the Web version of this article.)

Table 2
Summarized detrital zircon fission-data.

Sample	Tectonic block	Unit	Stratigraphic age	n	P(χ2) (%)	Dispersion (%)	Age range (Ma)	Peak 1 (age Ma_error _peak percent %)	Peak 2 (age in Ma/error/peak percent %)	Peak 3 (age in Ma/error/peak percent %)	Peak 4 (age in Ma/error/peak percent %)
AP-022	RFZ	Amagá Fm.	L. Oligocene- M. Miocene	94	0	45	21.3–358.8	**41.8**_4.3,+4.9_33 ± 6	**70.1**_-5.2,+5.6_58 ± 6	**144.9**/-17.4,+19.8/6 ± 6	**335.2**_-66.7, +82.8_4 ± 2.6
JM-050	WC	Penderisco Fm.	L.Campaniano-E. Maastrichtian	100	0	46	30.7–308.0	**57.1** _ −5.5,+6.1_23 ± 4	**104.3**_-8.6,+9.4_46 ± 6	**201.8**_ −18.1,+19.9_46 ± 6	–
JM-027	WC	Penderisco Fm.	L. Campaniano-E. Maastrichtian	95	0	50	40.4–487.7	**71.6**_-6.4,+7.0_31 ± 5	**132.8**_-11.5,+12.5_36 ± 6	**209.2**_-22.1,+24.7_30 ± 5	**377.9**_-51.0,+58.7_9 ± 3
SL-046	RFZ	Abejorral Fm.	Albiano-Aptiano	100	0	40	83.6–961.9	**128.2**_-12, +13.5_ 8 ± 3	**268.1**_18.4,+19.7_ 63.5 ± 5.5	**511.6**_-47.2, +51.8_28.2 ± 5.1	–

Sample coordinates are presented in Table S1 ζ = 135.1 ± 3.0 (A.P.).

(JM027 and JM050). These samples were collected west of the RFZ. From sample JM027, we dated 95 single zircon grains and obtained ages between 40.4 Ma and 487.7 Ma, uranium content is between 34.2 ppm and 410.4 ppm, and data dispersion of 50%. There are four distinct age populations at 71.6 Ma, 132.8 Ma, 209.2 Ma, and 377.9 Ma (Table 2; Fig. 3B and C). From sample JM050, we performed ZFT thermochronology on 100 single zircon grains, and the ages range between 30.7 Ma and 308.0 Ma, with uranium content between 45.5 ppm and 421.6 ppm, and data dispersion of 46%. There are three distinct age populations at 57.1, Ma, 104.3 Ma, and 201.8 Ma (Table 2; Fig. 3B and C).

5.1.6. *Amagá Formation (RFZ)*

ZFT thermochronology on 94 single grains from a sandstone sample from the Amagá Formation (AP-022) produced single grain ages between 21.2 Ma and 358.0 Ma, with uranium content between 20.0 and 271.9 ppm, and data dispersion of 45%. There are four distinct age populations at 41.8 Ma, 70.1 Ma, 144.9 Ma, and 335.2 Ma (Table 2; Fig. 3B and C).

5.2. *U-PB Zircon geochronology*

The sandstone sample from the Amagá Formation yielded ages that range between 78.7 Ma and 147.8 Ma, with age peaks at ~81 Ma, 86 Ma, 111 Ma, and 148 Ma (Fig. 4A). Analyzed zircons have subhedral and anhedral shapes with lengths between 100 and 300 μm and wide/length ratio of 2:3. The predominant internal texture of zircons are homogeneous and faint zoning; inheritance cores are absent.

6. Discussion

6.1. *Thermal and tectonic evolution of the Cretaceous sedimentary basins*

The two ZFT ages from Permo-Triassic granitoids in the RFZ suggest contrasting thermal histories. In the west, the Triassic ZFT age from the Pácora Stock (239.0 ± 11.0 Ma) is only 20 Ma younger than the U–Pb age (260.5 ± 4.7 Ma in Zapata et al., 2019a) (Figs. 3A and 5A), which reflects post-magmatic cooling or/and exhumation during the Triassic. In contrast, ZFT ages from the Abejorral Gneiss along the eastern RFZ reveal Cretaceous cooling at ~111 Ma. Lower Cretaceous detrital ZFT ages are present in the Abejorral Formation within the RFZ, sample SL046 has an age population of 128.2 Ma, which is slightly older than the stratigraphic age of this unit (Fig. 5A) (~125–100 Ma in Zapata et al., 2019a). This ZFT age population correlates with the volcanism coeval with the deposition of the Abejorral Formation between 125 and 100 Ma, (Zapata et al., 2019a). This age population may also be the result of the Cretaceous exhumation between 150 and 110 Ma documented in the Abejorral Gneiss and the Amagá Stock (Saenz, 2003) (Fig. 5A). However, this interpretation would require fast exhumation rates to transport rocks from below the ZPAZ to the surface in less than ~20 Ma.

The ZFT age peak at ~268 Ma in the Abejorral Formation (SL-046) is similar to the ZFT age obtained in the Pácora stock (239.0 ± 11 Ma) and the U–Pb zircon ages from the Abejorral Gneiss and the Pácora Stock (Fig. 5B) (Vinasco et al., 2006; Zapata et al., 2019a). These results suggest that the levels above the ZPAZ in the Pácora Stock and the Abejorral Gneiss were source areas for the sediments accumulated in the Abejorral Formation during the Cretaceous. This interpretation is consistent with published provenance studies from the Abejorral Formation, which based on U–Pb geochronology and heavy minerals have suggested that the Pácora Stock and the Abejorral Gneiss were part of their source areas (León et al., 2019; Zapata et al., 2019a).

Early Cretaceous ZFT data from the CC have been interpreted as products of deformation and exhumation promoted by the collision of an intra-oceanic volcanic arc (Quebradagrande Complex) with the continental margin (Spikings et al., 2015; Villagómez et al., 2011b). However, as discussed in detail in Zapata et al. (2019a), the stratigraphy and

Table 3
ZHe data.

Sample	Tectonic Block	Unit	Th (ppm)	U (ppm)	He (nmol/g)	ESR (μm)	eU (ppm)	Raw age (Ma)	Corrected Age (Ma)	1σ (Ma)	Mean age (Ma)
SZ-001	**RFZ**	Abejorral Gneiss	60.7	503.4	110.3	39.4	517.7	39.4	47.5	0.7	
			46.1	115.3	24.7	36.2	126.1	36.2	48.6	0.7	
			96.9	297.7	70.6	40.7	320.5	40.7	55	1.1	
			102.4	356.7	69.7	33.9	380.7	33.9	49	0.7	50.025
SZ-018	**CC**	Abejorral Fm. (andesitic lava)	61.65	166.4	42.5	101.9	180.9	43.4	49.6	1	
			30.69	64.1	14.3	39.4	71.4	37	53.2	1	
			28.04	81.4	17.2	48.4	88	36.2	48.4	1	
			25.49	73.8	16.3	56.1	79.8	37.8	48.4	1	49.9
JPC-013	**RFZ**	Quebradagrande Complex (andesitic lava)	106.32	220.3	57.9	43.6	245.2	43.6	55.1	0.7	
			93.41	194.8	48.3	41.2	216.7	41.2	51.3	0.7	
			214.76	435.1	113.5	43.2	485.6	43.2	59.4	1.1	
			245.92	374	106	45.3	431.8	45.3	62	0.8	56.95

Sample coordinates are presented in Table S1.
[1] Equivalent spherical radius.
[2] eU = [U]+0.235[Th], effective uranium content.

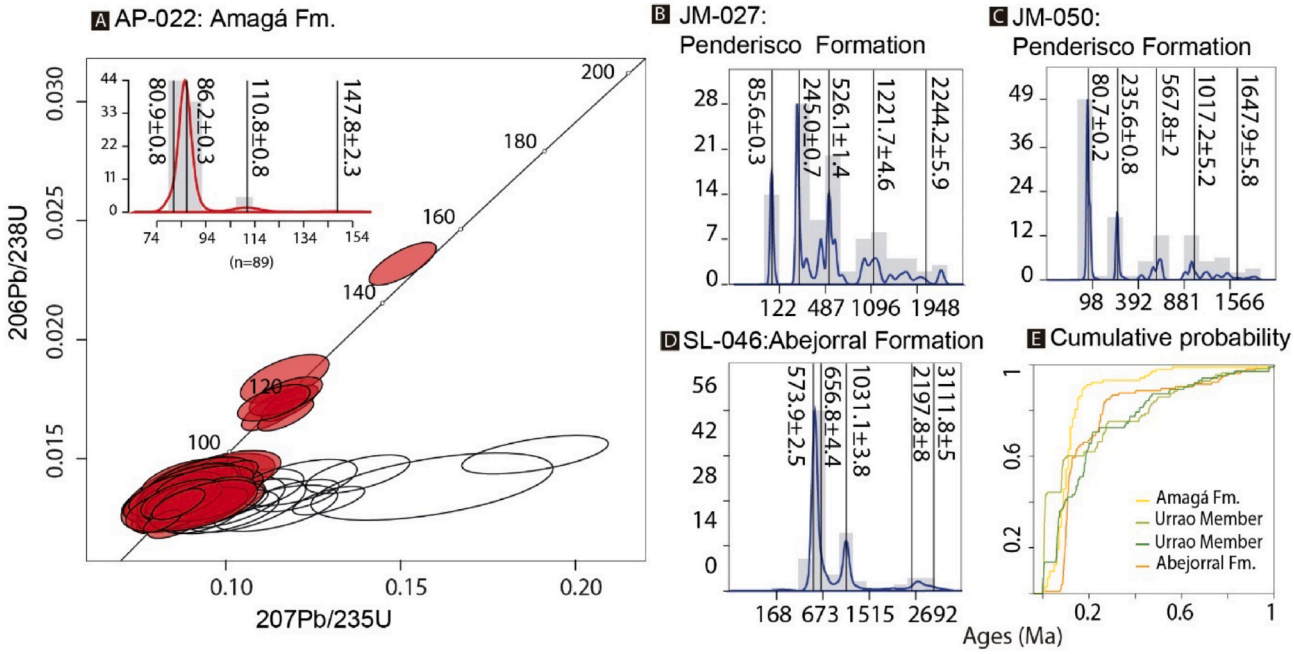

Fig. 4. A) U–Pb detrital zircon ages acquired in sample AP022 from the Amagá Formation. B–C) U–Pb detrital zircon ages acquired in the Penderisco Formation, modified from Pardo-Trujillo et al. (2020). U–Pb detrital zircon ages acquired in the Abejorral Formation, modified from Zapata et al. (2019a). E) Comparison of the cumulative probability curves.

the associated volcanism of the Abejorral Formation have more affinity with the development of a back-arc basin. Zapata et al. (2019a) and León et al. (2019) interpreted the Abejorral Gneiss as a horst block part of the Cretaceous back-arc basin, an interpretation based on the provenance of the Abejorral Formation, the associated volcanism, and the structural position of this unit. Moreover, new geochronology and geochemistry from the Quebradagrande Complex have conducted to new interpretations, in which these volcanic rocks were formed in the continental margin during the Late Cretaceous (Jaramillo et al., 2017; Zapata et al., 2019a). Therefore, the ZFT age of sample SZ-001 (~111 Ma) can be interpreted as a result of a footwall exhumation instead of collision (Fig. 6 A, B). Early Cretaceous Ar–Ar ages (127–100 Ma) from shear zones within the RFZ were previously interpreted as the age of deformation of several faults within the RFZ (Vinasco and Cordani, 2012). These ages were likely the expression of normal faulting and/or hydrothermal activity related to the magmatism recorded in the Abejorral Formation.

The Paleogene to Eocene ZHe data from the Abejorral Formation (SZ-018) and the Quebradagrande Complex (JPC-013) suggested that the RFZ and the western segment of the CC experienced temperatures above ZPRZ ~150 °C during the Late Cretaceous to Paleocene, these temperatures were required to fully reset ZHe ages after the accumulation of these units (Guenthner et al., 2013; Reiners, 2005). Based on the b-parameter of illite, León et al. (2019) suggested Early Cretaceous geothermal gradients between 25 and 35 °C/km. We used these geothermal gradients and a mean annual surface temperature of 15 °C to estimate that samples SZ-018 and JPC13 were overlain by at least ~4–5 km of Late Cretaceous to Early Paleocene strata. These findings suggested that the Late Cretaceous to Paleocene sedimentary strata could have been thicker than the strata preserved in the CC and the RFZ, which have been estimated at maximum values of ~2 km (Gómez-Cruz et al., 1995; González et al., 1988). Since the ZFT ages from sample SL046 were not reset, maximum burial temperatures never exceeded ~260 °C and thus, the sedimentary cover overlying these samples did not exceed 10 km. In this region deformation started around 90 Ma (Zapata et al., 2019a), thus, another plausible explanation is that crustal shortening

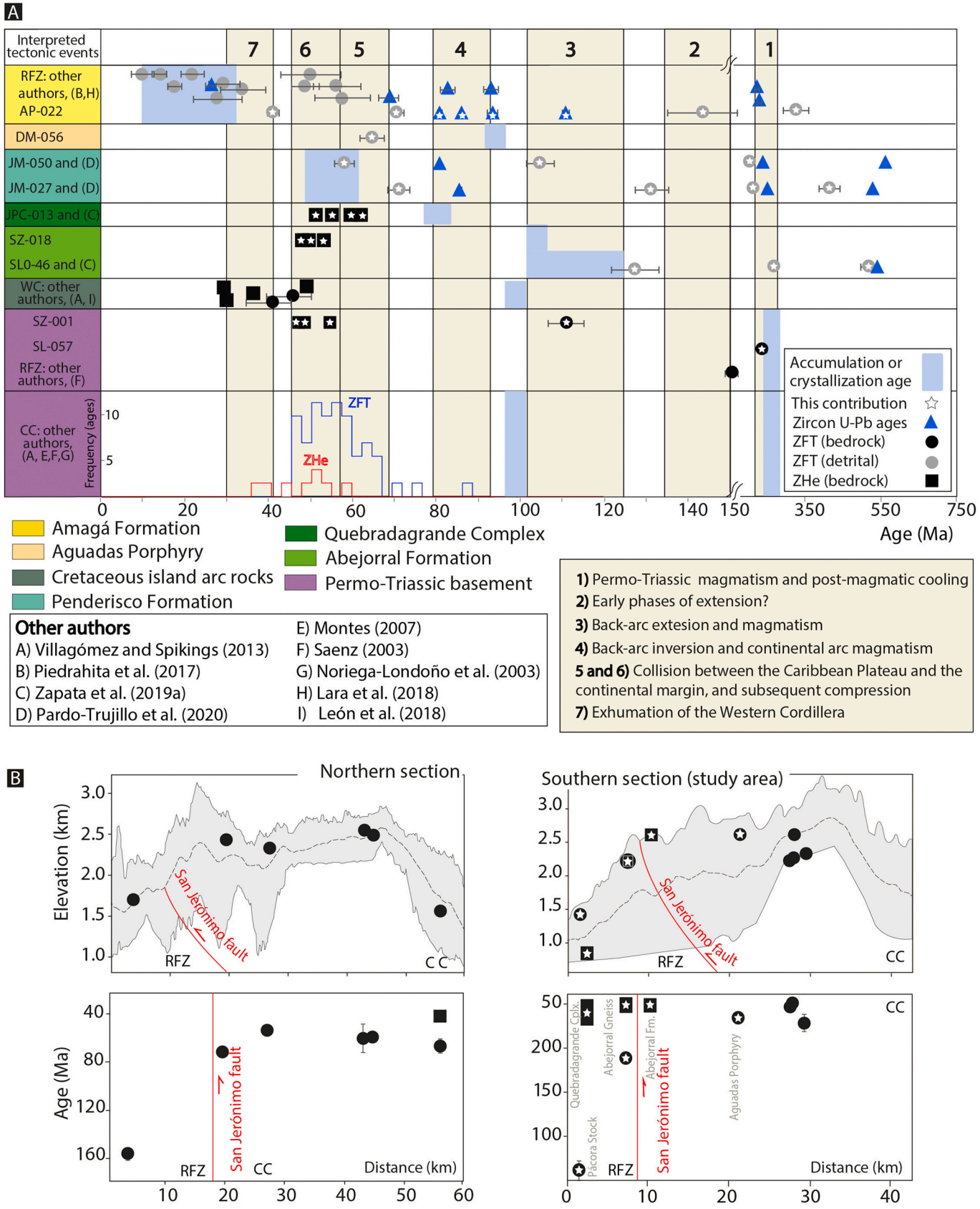

Fig. 5. A) Comparison between the ZFT data, zircon U–Pb age populations from the northern segments of the Romeral Fault Zone (RFZ), Central Cordillera (CC), and Western Cordillera (WC). U–Pb ages older than 600 Ma are not included because they don't overlap with the ZFT ages. Stars denote the data presented in this contribution. B) Topography of the studied section and one additional section located in a similar structural position farther north, available ZFT and ZHe are presented for each section, location is presented in Fig. 1.

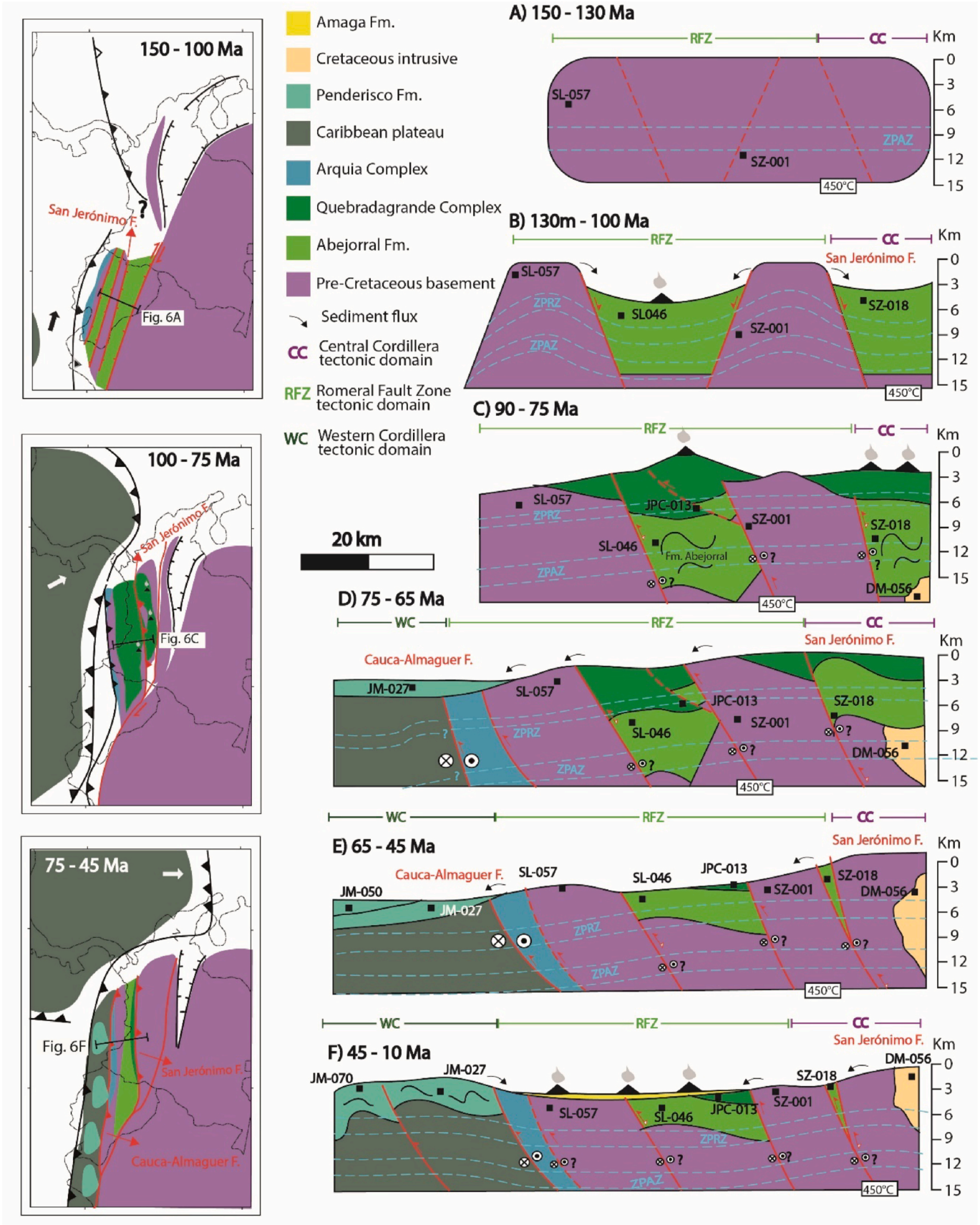

Fig. 6. Schematic model for the tectonic evolution of the study area. Paleogeography on the left panel is modified from Zapata et al. (2019a). The vertical scale was constructed using a thermal gradient of 30 °C/km (León et al., 2019). Light blue dashed lines denote the Zircon Partial Retention Zone (ZPRZ) and the Zircon Partial Annealing Zone (ZPAZ). Black squares denote the samples presented in this contribution. (For interpretation of the references to color in this figure legend, the reader is referred to the Web version of this article.)

increased the structural thickness above the Early Cretaceous strata (Fig. 6C).

6.2. Basin inversion and collision of the Caribbean Plateau

Our results documented two periods of cooling between the Late Cretaceous and the Eocene. ZHe ages between ~51 and 62 Ma from Sample JPC-013 from the Quebradagrande Complex suggest cooling below 150 °C during the Paleocene. The two aliquots with the highest eU values (>400 ppm) exhibited overlapping ages around 60 Ma, likely reflecting an increase in helium retentivity associated with radiation damage effects (Guenthner et al., 2013). In consequence, these older high eU ages recorded earlier stages of cooling within the RFZ. The two aliquots with relatively low eU values reflected a later stage of cooling around 51 Ma (Figs. 3D and 5A). East of the San Jerónimo Fault, ZFT data from the Aguadas Porphyry (DM-056) suggest cooling at ~65 Ma. This age together with the reported Late Cretaceous ZFT (Montes, 2007; Saenz, 2003) suggests that exhumation started in the Late Cretaceous in the CC, east of the San Jerónimo Fault (Figs. 5A and 6D).

Late Cretaceous to Paleocene cooling in the RFZ and the CC was coeval with the collision of the Caribbean oceanic plateau with the South American margin (Montes et al., 2019; Spikings et al., 2015; Villagómez et al., 2011b). Therefore, the Late Cretaceous to Paleogene cooling can be related to the inversion of the Cretaceous basins and the exhumation of the basement of the CC during such collision. The removal of the easily erodible Cretaceous sedimentary strata may have facilitated the fast exhumation of these units (Sobel and Strecker, 2003; Zapata et al., 2019b). East of the San Jerónimo Fault, on the western flank of the CC, ZHe data of the Abejorral Formation (SZ-018) suggest cooling at ~50 Ma (Fig. 5B). This cooling suggests ongoing exhumation associated to compression during the Eocene, after the collision of the Caribbean plateau.

We have integrated two different transects from the western flank of the CC, which included published ZFT and ZHe ages (Montes et al., 2015; Noriega-Londoño et al., 2020; Saenz, 2003; Villagómez and Spikings, 2013), and new data in this study (Fig. 5B). In these transects, west of the San Jerónimo Fault, the Abejorral Gneiss (Sample SZ-001), Pácora Stock (Sample SL-057), and Amagá Stock (Saenz, 2003) exhibit ZFT ages older than ~110 Ma. In contrast, east of the San Jerónimo Fault, ZFT ages are between 65 and 50 Ma (Figs. 1 and 5B). In these transects, youngest ZFT ages are located at higher elevations, in the hanging wall of the San Jerónimo. This difference in the ZFT ages suggests differential exhumation between the foot and hanging wall of the San Jerónimo Fault. These differences in ZFT ages required at least ~3 km of more rock uplift east of the San Jerónimo Fault to transport rocks trough the ZPAZ (~350 °C–250 °C) during the Paleocene. Tectonic rock uplift in the hanging wall of the San Jerónimo Fault promoted erosion and, thus, the exhumation of the CC basement. Exhumation along the San Jerónimo Fault continued during the Paleogene, as suggested by Eocene ZHe ages in the core of the Cordillera (Montes et al., 2015; Noriega-Londoño et al., 2020; Saenz, 2003).

These results indicate that the San Jerónimo Fault accommodated most of the Paleogene compression and controlled the onset of the uplift of the CC. During the Paleogene, the upper segments the Late Cretaceous volcanic arc were fully eroded and thus deeper crustal levels such as the Aguadas Porphyry and the Antioquia Batholith were exposed (Fig. 6E and F). The less Paleogene exhumation in the footwall of the San Jerónimo Fault (RFZ) favored the preservation of older ZFT ages and the volcanoclastic rocks of the Quebradagrande Complex, which constitutes the more superficial levels of the Late Cretaceous volcanic arc that formed the Antioquia Batholith (Fig. 6C). Therefore, the Quebradagrande Complex could have been the surface expression of the plutonism that formed the Antioquia Batholith.

Samples JM-027 and JM-050 from the Late Cretaceous-Paleocene Penderisco Formation were collected in different structural positions across the strike of the WC (Fig. 1). These samples produced U–Pb maximum depositional ages of 79.4 ± 0.8 Ma and 72.9 ± 0.8 Ma, respectively (Fig. 4B and C) (Pardo-Trujillo et al., 2020). Sample JM-027 yielded similar ZFT and U–Pb maximum depositional ages (ZFT: ~71 Ma, U–Pb: ~80 Ma), suggesting a Late Cretaceous accumulation of this unit. In contrast, the younger ZFT age population peak from the age distribution of sample JM-050 (57.7 Ma) was significantly younger than the U–Pb maximum depositional age. A plausible explanation is that this younger population is the result of partial resetting, this would imply a thick sedimentary cover and/or high thermal gradients. However, this sample does not show a clear relation between young ZFT ages and high uranium content (Fig. 3B), which can be an indicator of partial resetting due to lower resistance to annealing of grains with radiation damage effects (Bernet et al., 2009). Moreover, the thickness of the Penderisco Formation is not constrained and the relative position of the samples before deformation is unknown. Thus, we favor the interpretation in which some segments of the Penderisco Formation were deposited during the Late Paleocene-Eocene (Pardo-Trujillo et al., 2020). The lack of Paleocene U–Pb zircon ages in sample JM-050 (Fig. 4C) would suggest that these Paleocene ZFT ages were more likely to be the result of the documented Paleocene exhumation of the CC rather than Paleocene volcanism.

The maximum ZFT depositional ages of both samples (57.1 Ma and 71.6 Ma) are consistent with the Late Cretaceous to Eocene cooling and magmatic events documented in the RFZ and the CC (Fig. 5A). Both samples have Cretaceous ZFT age populations of 104 Ma and 133 Ma and older Triassic populations of ~202 Ma and 209 Ma (Fig. 3C), which were characteristic of the CC and the RFZ (Fig. 5A). Thus, we have interpreted the Penderisco Formation as a sedimentary succession accumulated during the deformation and progressive unroofing of the RFZ and the CC during and after the collision with the Caribbean Plateau. Furthermore, during the Paleocene, the CC was a positive relief feature and constituted the main source area of the Penderisco Formation This conclusion agrees with previous interpretations and provenance data presented by Pardo-Trujillo et al. (2020).

6.3. Late eocene to miocene, the formation of an intermountain basin

Oligocene to Eocene apatite fission-track (AFT) ages suggest that during this time interval the CC continued cooling (Noriega Londoño, 2016; Villagómez and Spikings, 2013). Moreover, the absence of Eocene sediments suggests that the RFZ and the CC remained as positive elements during this time interval. Eocene to Oligocene ZFT and AFT ages from the WC may represent the onset of rock uplift in the WC and thus the formation of an intermountain basin in the RFZ (León et al., 2018; Villagómez and Spikings, 2013).

The U–Pb age populations at 81 Ma and 86 Ma in a sandstone from the Amagá Formation (Fig. 4A) coincided with magmatic crystallization ages from volcanic and plutonic lithologies associated with the Quebradagrande Complex (Jaramillo et al., 2017; Montes et al., 2019). The age population peak at ~111 Ma coincided with the crystallization ages of magmatic rocks from the Abejorral Formation (Fig. 5A; Zapata et al., 2019a). Relatively old maximum depositional ages in the study area are similar to the ages reported in the basal levels of the Amagá Formation farther north (Lara et al., 2018b), which suggest deposition before the onset of Miocene volcanism. ZFT cooling signatures suggested deposition after ~42 Ma for this segment of the Amagá Formation. This younger age population was likely related to exhumation and/or magmatism during the onset of deformation in the WC (Figs. 5A and 6F) (León et al., 2018). The ZFT age peak at ~70 Ma was probably sourced from the Late Cretaceous magmatism preserved in the CC and the RFZ, and/or the deformation and erosion of the Penderisco Formation in the WC (Fig. 5A). The ZFT age peak at ~145 Ma was sourced either from the Penderisco Formation and/or the Lower Cretaceous horst remnants preserved within the RFZ. We interpreted that the strata from the Amagá Formation preserved in the study area was sourced from both WC and CC. The accumulation of this unit marks the onset of sedimentation after

the formation of an intermountain basin (Fig. 6F). Farther north within the RFZ, the Amagá Formation exhibit ZFT ages between 60 and 10 Ma, younger ages are the result of Miocene magmatism in younger segments of the Amagá Formation while Late Cretaceous to Eocene was sourced from the both CC and WC.

6.4. Implication for the tectonic evolution of the Northern Andes

Our results agreed with the initial observation made by Zapata et al. (2019a) based on U–Pb data, herein, despite the Cretaceous to Cenozoic strike-slip deformation along NW South American, major kilometric strike-slip displacements are not necessary to explain the detrital ZFT ages from the Cretaceous to Miocene sedimentary units from the WC, the RFZ, and the CC (Fig. 5A). In our data set, Paleocene to Eocene ZFT ages characteristic of the CC are present in all detrital ZFT age distributions from Cretaceous to Miocene sedimentary units in the RFZ and the WC, suggesting that these tectonic blocks remained connected between the Cretaceous and Miocene. Therefore, plate scale kilometric fault displacements are not necessary to explain the tectonic evolution of these units. We acknowledge that the lack of thermochronological data in the southern segment of the CC is a limitation for the interpretation of our data and more precise correlations.

The Late Cretaceous to Cenozoic uplift and deformation of the CC promoted the erosion of the overlying sedimentary cover and upper crustal levels. The absence of stratigraphic makers within this mountain range has difficulted the correlation with the adjacent tectonic blocks and difficulted the reconstruction of vertical fault displacements. This study shows how combined bedrock and detrital thermochronology can constraint thick-skin deformation in basement rocks older than the deformational phases. Similar approaches to understand thick-skin deformation have been successfully conducted in other segments of the Andes, such as the Sierras Pampeanas and the Eastern Cordillera of Colombia (e.g. Löbens et al., 2013; Nemčok et al., 2013; Zapata et al., 2020).

The San Jerónimo fault has been suggested as a major terrane boundary in the Northern Andes (Restrepo and Toussaint, 2020, 1988). However, several authors have shown that the Quebradagrande Complex has a magmatic record coeval with the emplacement of the Antioquia Batholith (Jaramillo et al., 2017; Zapata et al., 2019a). Our study has documented the differential exhumation of the blocks east and west of the San Jerónimo Fault, which suggests that Cenozoic rock uplift and exhumation focused on the CC. Consequently, we propose that the metamorphic and igneous basement of the CC represents a deep crustal section of the Late Cretaceous volcanic arc. In contrast, west of the San Jerónimo fault, the volcanoclastic rocks from Quebradagrande Complex represent the remnants of the upper segment of the same volcanic arc; these volcanoclastic rocks were preserved due to the relatively lower exhumation of Cenozoic exhumation within the RFZ. Therefore, between 5 and 7 °N the San Jerónimo Fault does not represent a major terrane boundary. The Cauca-Almaguer Fault represents a terrane limit between the Caribbean Plateau and the continental margin. However, the provenance of the Penderisco Formation suggests that the CC and the WC remained connected after the collision (Pardo-Trujillo et al., 2020).

This study does not neglect the presence of a strike-slip component in the San Jerónimo and Cauca Almaguer Faults, which has been widely documented (Vinasco and Cordani, 2012). However, our model suggests that: (1) the San Jerónimo fault accommodate significant vertical movement during the Cenozoic, (2) the WC, the RFZ, and the CC have been connected since the Early Cretaceous, and (3) no kilometric displacements along the margin are necessary to explain the provenance of the sedimentary units in the study area or the presence of different crustal levels (e.g. volcanic vs plutonic) limited by such faults. Thus, major strike-slip displacements between these tectonic blocks can not be inferred from the available data. This conclusion does not preclude minor strike-slip displacements, which can not be inferred from basin-scale provenance or basement thermochronology. Our study highlights the importance of differential exhumation to define terrane limits and interpret the transgressional accretionary history of the Northern Andes.

7. Conclusions

This study presented new detrital and bedrock ZHe and ZFT ages for the units between the Central and Western Cordilleras. As a result, we have refined the thermal evolution of the Cretaceous basins that developed in the western segment of the Northern Andes. A thick volcano-sedimentary succession related to the formation of a Late Cretaceous volcanic-arc unconformably overlies the RFZ and the west of the CC. The San Jerónimo fault, which has been interpreted as a major terrane boundary, it's suggested to be the limit between two different segments of the same volcanic arc; this fault accommodated most of the Paleogene deformation and controlled the uplifting of the Central Cordillera, which was a positive relief element during the Cenozoic. Finally, the Amagá Formation recorded the onset of Eocene to Oligocene sedimentation after the uplift of the Western Cordillera and the formation of an intermountain basin.

Declaration of competing interest

The authors declare that they have no known competing financial interests or personal relationships that could have appeared to influence the work reported in this paper.

CRediT authorship contribution statement

S. Zapata: Conceptualization, Investigation, Project administration, Writing - review & editing. **A. Patiño:** Conceptualization, Investigation, Formal analysis, Writing - review & editing. **A. Cardona:** Conceptualization, Investigation, Supervision, Writing - review & editing, Resources. **M. Parra:** Conceptualization, Formal analysis, Investigation, Writing - review & editing, Resources. **V. Valencia:** Formal analysis, Investigation, Resources. **P. Reiners:** Formal analysis, Investigation, Resources. **F. Oboh-Ikuenobe:** Conceptualization, Funding acquisition, Writing - review & editing. **F. Genezini:** Formal analysis.

Acknowledgments

We acknowledge the support for S. Zapata from the MST-STRI Bytnar Postdoctoral Fellowship. Funding from the National University of Colombia projects 25452, 25340, 29182, 18593, 24208, and the Fundación para la Promoción de la Investigación y la Tecnología del Banco de la República de Colombia, project3451, and the Sao Paulo Research Foundation (FAPESP) JP grant 2013-03265-5. Colleagues from the EGEO research group at the National University of Colombia are acknowledged for their discussions. Maria Isabel Marín from EAFIT University (Medellín, Colombia) is acknowledged for allowing access to the Thermochronology Laboratory. German Bayona and Matthias Bernet are acknowledged for their valuable comments during the review of this manuscript.

Appendix A. Supplementary data

Supplementary data to this article can be found online at https://doi.org/10.1016/j.jsames.2020.102715.

References

Amaya, C., Centenaro, J., 1997. Ambiente deposicional y modelamiento delYacimiento Caballos en el Campo Orito, Cuenca Putumayo. 6 Simp. Bol.Expl. Pet. En las Cuencas Subandinas 2, 30–33.

Amaya, S., Zuluaga, C.A., Bernet, M., 2017. New fission-track age constraints on the exhumation of the central Santander Massif: implications for the tectonic evolution

of the Northern Andes, Colombia. Lithos 282–283, 388–402. https://doi.org/10.1016/j.lithos.2017.03.019.
Avellaneda-Jiménez, D.S., Cardona, A., Valencia, V., Barbosa, J.S., Jaramillo, J.S., Monsalve, G., Ramírez-Hoyos, L., 2019. Erosion and regional exhumation of an Early Cretaceous subduction/accretion complex in the Northern Andes. Int. Geol. Rev. https://doi.org/10.1080/00206814.2019.1596042.
Bayona, G., Cardona, A., Jaramillo, C., Mora, A., Montes, C., Valencia, V., Ayala, C., Montenegro, O., Ibañez-Mejia, M., 2012. Early Paleogene magmatism in the northern Andes: insights on the effects of oceanic plateau–continent convergence. Earth Planet Sci. Lett. 331, 97–111.
Bernet, M., 2009. A field-based estimate of the zircon fission-track closure temperature. Chem. Geol. 259, 181–189.
Bernet, M., Brandon, M., Garver, J., Balestieri, M.L., Ventura, B., Zattin, M., 2009. Exhuming the Alps through time: clues from detrital zircon fission-track thermochronology. Basin Res. 21, 781–798. https://doi.org/10.1111/j.1365-2117.2009.00400.x.
Bernet, M., Garver, J.I., Bernet, M., Fission-track, J.I.G., 2006. Fission-track analysis of detrital zircon. To Cite This Version : HAL Id : Hal-00097116 205–238.
Brandon, M.T., 1996. Probability density plot for fission-track grain-age samples. Radiat. Meas. 26, 663–676.
Brandon, M.T., Roden-Tice, M.K., Garver, J.I., 1998. Late cenozoic exhumation of the cascadia accretionary wedge in the olympic mountains, northwest Washington state. Geol. Soc. Am. Bull. 110, 985–1009.
Broussolle, A., Sun, M., Schulmann, K., Guy, A., Aguilar, C., Štípská, P., Jiang, Y., Yu, Y., Xiao, W., 2019. Are the Chinese Altai "terranes" the result of juxtaposition of different crustal levels during Late Devonian and Permian orogenesis? Gondwana Res. 66, 183–206.
Bustamante, A., Juliani, C., Essene, E.J., Hall, C.M., Hyppolito, T., 2011. Geochemical constraints on blueschist- and amphibolite-facies rocks of the Central Cordillera of Colombia: the Andean Barragán region. Int. Geol. Rev. 54, 1013–1030. https://doi.org/10.1080/00206814.2011.594226.
Caballero, V., Parra, M., Mora, A., López, C., Rojas, L.E., Quintero, I., 2013. Factors controlling selective abandonment and reactivation in thick-skin orogens: a case study in the Magdalena Valley, Colombia. Geol. Soc. London, Spec. Publ. 377, 343–367. https://doi.org/10.1144/sp377.4.
Cardona, A., León, S., Jaramillo, J.S., Valencia, V., Zapata, S., Pardo–Trujillo, A., Schmitt, A.K., Mejía, D., Arenas, J.C., 2019. Cretaceous record from a mariana to an andean–type margin in the central cordillera of the Colombian Andes. In: Gómez, J., Pinilla–Pachon, A. (Eds.), The Geology of Colombia, ume 2. Servicion Geologico Colombiano, Publicaciones Geológicas Especiales, Bogota, pp. 353–395. https://doi.org/10.32685/pub.esp.36.2019.1.
Cardona, A., Montes, C., Ayala-Calvo, C., Bustamante, C., Hoyos, N., Montenegro, O., Ojeda, C., Niño, H., Ramirez, V., Rincon, D., Vervoort, J.D., Zapata, S., 2012. From arc-continent collision to continuous convergence, clues from Paleogene conglomerates along the southern Caribbean-South America plate boundary. Tectonophysics 580, 58–87.
Cardona, A., Valencia, V., Weber, M., Duque, J., Montes, C., Ojeda, G., Reiners, P., Domanik, K., Nicolescu, S., Villagomez, D., 2011. Transient Cenzoic tectonic stages in the southern margin of the Caribbean plate: U-Th/He thermochronological constraints from Eocene plutonic rocks in the Santa Marta Massif and Serranía de Jarara, northern Colombia. Geol. Acta 9, 445–466. https://doi.org/10.1344/105.000001739.
Cetina, L.M., Celso, C., Tassinari, G., García, G.R., Restrepo, T.C., 2019. Origin of pre-mesozoic xenocrystic zircons in cretaceous sub-volcanic rocks of the northern Andes (Colombia): paleogeographic implications for the region. J. South Am. Earth Sci. 102363 https://doi.org/10.1016/j.jsames.2019.102363.
Chang, Z., Vervoort, J.D., McClelland, W.C., Knaack, C., 2006. U-Pb dating of zircon by LA-ICP-MS. G-cubed 7, 1–14.
Dodson, M.H., 1973. Closure temperature in cooling geochronological and petrological systems. Contrib. Mineral. Petrol. 40, 259–274. https://doi.org/10.1007/BF00373790.
Dumitru, T.A., 1993. A new computer-automated microscope stage system for fission-track analysis. Nucl. Tracks Radiat. Meas. 21, 575–580.
Duque-Trujillo, J., Bustamante, C., Solari, L., Gómez-Mafla, Á., Toro-Villegas, G., Hoyos, S., 2019. Reviewing the Antioquia batholith and satellite bodies: a record of Late Cretaceous to Eocene syn- to post-collisional arc magmatism in the Central Cordillera of Colombia. Andean Geol. 46, 82–101.
Flowers, R.M., 2009. Exploiting radiation damage control on apatite (U – Th)/He dates in cratonic regions. Earth Planet Sci. Lett. 277, 148–155. https://doi.org/10.1016/j.epsl.2008.10.005.
Flowers, R.M., Kelley, S.A., 2011. Interpreting data dispersion and " inverted " dates in apatite (U – Th)/He and fission-track datasets : an example from the US midcontinent. Geochem. Cosmochim. Acta 75, 5169–5186. https://doi.org/10.1016/j.gca.2011.06.016.
Galbraith, R.F., Laslett, G.M., 1993. Statistical models for mixed fission track ages. Nucl. Tracks Radiat. Meas. 21, 459–470.
Gallagher, K., Brown, R., Johnson, C., 2002. Fission track analysis and its applications to geological problems. Annu. Rev. Earth Planet Sci. 26, 519–572. https://doi.org/10.1146/annurev.earth.26.1.519.
García-Ramírez, C.A., Ríos-Reyes, C.A., Castellanos-Alarcón, O.M., Mantilla-Figueroa, L. C., 2017. Petrology, geochemestry and geochronology of the arqui complex metabasites at the pijao-genove sector, central cordillera, Colombian Andes. Bol. Geol. 39, 105–126.
Gehrels, G., Valencia, V., Pullen, A., 2006. Detrital zircon geochronology by laser-ablation multicollector ICPMS at the Arizona laserchron center. Geochronol. Emerg. Oppor. Paleontol. Soc. Short Course 11, 67–76. https://doi.org/10.1002/9781444347166.ch2. Oct. 21, 2006, Philadelphia, PA. Paleontol. Soc. Pap.
Gómez-Cruz, A., Moreno Sánchez, M., Pardo-Trujillo, A., 1995. Edad y Origen del "Complejo metasedimentario Aranzazu-Manizales" en los Alrededores de Manizales (Departamento de Caldas, Colombia). Geol. Colomb. 19, 83–93.
Gleadow, A.J.W., Hurford, J., Quaife, R.D., 1976. Fission track dating of zircon: improved etching techniques. Earth Planet. Sci. Lett. 33 (2), 273–276.
Gómez, J., Nivia, Á., Montes, N.E., Almanza, M.F., Alcárcel, F.A., Madrid, C., 2015. Notas explicativas: mapa Geológico de Colombia. Compil. la Geol. Colomb. Una visión a 9–33.
González, H., 2001. Mapa geológico de Antioquia escala 1: 400.000. Memoria Explicativa. Ingeominas. Bogotá.
González, H., Nuñez, A., Paris, G., 1988. Mapa geologico de Colombia, 1: 1 500 000 1988: memoria explicativa. Instituto Nacional de Investigacionnes Geologico-Mineras.
Green, P.F., 1981. A new look at statistics in fission-track dating. Nucl. Tracks 5, 77–86. https://doi.org/10.1016/0191-278X(81)90029-9.
Guenthner, W.R., Reiners, P.W., Ketcham, R.A., Nasdala, L., Giester, G., 2013. Helium diffusion in natural zircon: radiation damage, anisotropy, and the interpretation of zircon (U-Th)/He thermochronology. Am. J. Sci. https://doi.org/10.2475/03.2013.01.
Guy, A., Schulmann, K., Soejono, I., Xiao, W., 2020. Revision of the Chinese altai-east junggar terrane accretion model based on geophysical and geological constraints. Tectonics 39, e2019TC006026.
Harrison, T.M., 2005. Fundamentals of noble gas Thermochronometry. Rev. Mineral. Geochem. 58, 123–149. https://doi.org/10.2138/rmg.2005.58.5.
Hincapié-Gómez, S., Cardona, A., Jiménez, G., Monsalve, G., Ramírez-Hoyos, L., Bayona, G., 2018. Paleomagnetic and gravimetrical reconnaissance of cretaceous volcanic rocks from the western Colombian Andes: paleogeographic connections with the Caribbean plate. Studia Geophys. Geod. 62, 485–511.
Horton, B.K., Saylor, J.E., Nie, J., Mora, A., Parra, M., Reyes-Harker, A., Stockli, D.F.E., 2010. Linking sedimentation in the northern Andes to basement configuration, Mesozoic extension, and Cenozoic shortening: evidence from detrital zircon U-Pb ages, Eastern Cordillera, Colombia. Bull. Geol. Soc. Am. 122, 1423–1442. https://doi.org/10.1130/B30118.1.
Jaramillo, J.S., Cardona, A., Leon, S., Valencia, V., Vinasco Vallejo, C., 2017. Geochemistry and geochronology from cretaceous magmatic and sedimentary rocks at 6°35′ n, Western flank of the Central Cordillera (Colombian Andes): magmatic record of arc growth and collision. J. South Am. Earth Sci. 76, 460–481.
Kerr, A.C., Marriner, G.F., Tarney, J., Nivia, A., Saunders, A.D., Thirlwall, M.F., Sinton, C. W., 1997. Cretaceous basaltic terranes in Western Colombia: elemental, chronological and Sr–Nd Isotopic Constraints on petrogenesis. J. Petrol. 38, 677–702.
Kerr, A.C., Tarney, J., 2005. Tectonic evolution of the Caribbean and northwestern South America: the case for accretion of two Late Cretaceous oceanic plateaus. Geology 33, 269–272. https://doi.org/10.1130/G21109.1.
Lara, M., Salazar-Franco, A.M., Silva-Tamayo, J.C., 2018a. Provenance of the cenozoic siliciclastic intramontane Amagá Formation: implications for the early Miocene collision between central and south America. Sediment. Geol. https://www.sciencedirect.com/science/article/abs/pii/S0037073818301544.
Lara, M., Salazar-Franco, A.M., Silva-Tamayo, J.C., 2018b. Provenance of the cenozoic siliciclastic intramontane Amagá Formation: implications for the early Miocene collision between central and south America. Sediment. Geol. 373, 147–162. https://doi.org/10.1016/j.sedgeo.2018.06.003.
Leal-Mejia, H., 2011. Phanerozoic Gold Metallogeny in the Colombian Andes: A Tectono-Magmatic Approach.
Leal-Mejía, H., Shaw, R.P., i Draper, J.C.M., 2019. Spatial-temporal migration of granitoid magmatism and the Phanerozoic tectono-magmatic evolution of the Colombian Andes. Geology and Tectonics of Northwestern South America. Springer, pp. 253–410.
León, S., Cardona, A., Mejía, D., Botello, G.E.E., Villa, V., Collo, G., Valencia, V., Zapata, S., Avellaneda-Jiménez, D.S.S., 2019. Source area evolution and thermal record of an Early Cretaceous back-arc basin along the northwesternmost Colombian Andes. J. South Am. Earth Sci. 94 https://doi.org/10.1016/j.jsames.2019.102229.
León, S., Cardona, A., Parra, M., Sobel, E.R., Jaramillo, J.S., Glodny, J., Valencia, V.A., Chew, D., Montes, C., Posada, G., Monsalve, G., Pardo-Trujillo, A., 2018. Transition from collisional to subduction-related regimes: an example from Neogene Panama-Nazca-South America interactions. Tectonics 37, 119–139. https://doi.org/10.1002/2017TC004785.
Löbens, S., Sobel, E.R., Bense, F.A., Wemmer, K., Dunkl, I., Siegesmund, S., 2013. Refined exhumation history of the northern Sierras Pampeanas, Argentina. Tectonics 32, 453–472. https://doi.org/10.1002/tect.20038.
Malusà, M.G., Fitzgerald, P.G., 2019. Application of thermochronology to geologic problems: bedrock and detrital approaches. Fission-Track Thermochronology and its Application to Geology. Springer, pp. 191–209.
Malusà, M.G., Garzanti, E., 2019. The sedimentology of detrital thermochronology. Fission-Track Thermochronology and its Application to Geology. Springer, pp. 123–143.
Maya, M., Gonzalez, H., 1995. Unidades litodemicas de la Cordillera central. Informe Unidad Operativa Medellin, pp. 44–57. Ingeominas.
Montes, C., Cardona, A., Jaramillo, C., Pardo, A., Silva, J.C.C., Valencia, V., Ayala, C., Pérez-Angel, L.C., Rodriguez-Parra, L.A., Ramirez, V., Niño, H., 2015. Middle Miocene closure of the central American seaway. Science 84 348, 226–229. https://doi.org/10.1126/science.aaa2815.
Montes, C., Rodriguez-Corcho, A.F., Bayona, G., Hoyos, N., Zapata, S., Cardona, A., 2019. Continental margin response to multiple arc-continent collisions : the northern

Andes-Caribbean margin. Earth Sci. Rev. 198, 102903. https://doi.org/10.1016/j.earscirev.2019.102903.
Montes, L.F., 2007. Exhumación de las rocas metamórficas de alto grado que afloran al oriente del valle del Aburrá. Universidad Eafit.
Mora, A., Baby, P., Roddaz, M., Parra, M., Brusset, 2010. In: Hoorn, C., Wesselingh, F.P. (Eds.), Tectonic History of the Andes and Sub Andean Zones: Implications for the Development of the Amazon Drainage Basin Amaz. Landsc. Species Evol. A Look into Past, Blackwell vol. 388, pp. 115–127.
Mora, A., Horton, B.K., Mesa, A., Rubiano, J., Ketcham, R.A., Parra, M., Blanco, V., Garcia, D., Stockli, D.F., 2019. Migration of Cenozoic Deformation in the Eastern Cordillera of Colombia Interpreted from Fission Track Results and Structural Relationships : Implications for Petroleum Systems. https://doi.org/10.1306/01051009111.
Murray, K.E., Braun, J., Reiners, P.W., 2018. Toward robust interpretation of low-temperature thermochronometers in magmatic terranes. G-cubed 19, 1–25. https://doi.org/10.1029/2018GC007595.
Naeser, C.W., Faul, H., 1969. Fission track annealing in apatite and sphene. J. Geophys. Res. 74 (2), 705–710.
Nemčok, M., Mora, A., Cosgrove, J., 2013. Thick-skin-dominated orogens; from initial inversion to full accretion: an introduction. Geol. Soc. London, Spec. Publ. 377, 1–17. https://doi.org/10.1144/sp377.17.
Noriega-Londoño, S., Restrepo-Moreno, S.A.A., Vinasco, C., Bermúdez, M.A.A., Min, K., 2020. Thermochronologic and geomorphometric constraints on the cenozoic landscape evolution of the northern Andes: northwestern central cordillera, Colombia. Geomorphology 351. https://doi.org/10.1016/j.geomorph.2019.106890.
Noriega Londoño, S., 2016. Geomorfología tectónica del noroccidente de la Cordillera Central , Andes del Norte - Colombia Geomorfología tectónica del noroccidente de la Cordillera Central. Andes del Norte - Colombia 151pp.
Pardo-Trujillo, A., Cardona, A., Giraldo, A.S., León, S., Vallejo, D.F., Trejos-Tamayo, R., Plata, A., Ceballos, J., Echeverri, S.1.5, Barbosa-Espitia, A., Slattery, J., Salazar, A., Botello, G.E., Celis, S.A., Osorio-Granad, C.A., 2020. Sedimentary record of the Cretaceous–Paleocene arc–continent collision in the northwestern Colombian Andes: insights from stratigraphic and provenance constraints. Sediment. Geol. 401, 105627.
Parra, M., Mora, A., Sobel, E.R., Strecker, M.R., González, R., 2009. Episodic orogenic front migration in the northern Andes: constraints from low-temperature thermochronology in the Eastern Cordillera, Colombia. Tectonics 28. https://doi.org/10.1029/2008TC002423.
Pearson, D.M., Kapp, P., DeCelles, P.G., Reiners, P.W., Gehrels, G.E., Ducea, M.N., Pullen, A., 2013. Influence of pre-Andean crustal structure on Cenozoic thrust belt kinematics and shortening magnitude: northwestern Argentina. Geosphere 9, 1766–1782. https://doi.org/10.1130/GES00923.1.
Reiners, P.W., 2005. Zircon (U-Th)/He Thermochronometry. Reiners, P.W. In: Ehlers, T. A. (Ed.), Thermochronology. Rev. Mineral. Geochemistry, vol. 58, pp. 151–176.
Reiners, P.W., Brandon, M.T., 2006. Using thermochronology to understand orogenic erosion. Annu. Rev. Earth Planet Sci. 34, 419–466. https://doi.org/10.1146/annurev.earth.34.031405.125202.
Reiners, P.W., Zeitler, P., 2005. Past, present, and future of thermochronology. Rev. Mineral. Geochem. 58, 1–18. https://doi.org/10.2138/rmg.2005.58.1.
Restrepo, J.J., Toussaint, J.F., 2020. Tectonostratigraphic terranes in Colombia: an update, first part: continental terranes. In: Gómez, J., Mateus–Zabala, D. (Eds.), The Geology of Colombia. Servicio Geológico Colombiano, Publicaciones Geológicas Especiales, Bogotá, pp. 45–95.
Restrepo, J.J., Toussaint, J.F., 1991. Terranes and continental acretion in the Colombian Andes. Episodes 11 (3), 189–193.
Restrepo, J.J., Toussaint, J.F., 1988. Terranes and continental accretion in the Colombian Andes. J. Int. Geosci. 11, 189–193.
Rodríguez, C., Rojas, R., 1985. Estratigrafía y tectónica de la serie infracretácica en los alrededores de San Félix, Cordillera Central de Colombia. Proy. Cretácico 16.
Rodriguez, G., Zapata, G., 2013. Comparative analysis of the Barroso Formation and Quebradagrande Complex: a volcanic arc tholeiitic–calcoalcaline, segmented by the fault system Romeral in Northern Andes. Bol. Ciencias la Tierra 33, 39–58.
Saenz, E.A., 2003. Fission track thermochronology and denudational response to tectonics in the north of the Colombian Central Cordillera. Masterthesis. Shimane Univ. S019221.
Sierra Lopera, G.M., Marín Cerón, M.I., Macdonald, W., 2012. Tectonic evolution of the irra pull-apart basin evidences of slip reversals on the romeral fault zone, northern part of andean central cordillera, Colombia. Boletín Ciencias la Tierra 32, 143–159.
Silva-Tamayo, J.C., Sierra, G.M., Correa, L.G., Silva, J., Sierra, G.M., Correa, L.G., Tamayo, J.C.S., Sierra, G.M., Correa, L.G., 2008. Tectonic and climate driven fluctuations in the stratigraphic base level of a Cenozoic continental coal basin, northwestern Andes. J. South Am. Earth Sci. 26, 369–382. https://doi.org/10.1016/j.jsames.2008.02.001.
Sobel, E.R., Chen, J., Heermance, R.V., 2006a. Late oligocene-early Miocene initiation of shortening in the southwestern Chinese tian Shan: implications for Neogene shortening rate variations. Earth Planet Sci. Lett. 247, 70–81. https://doi.org/10.1016/j.epsl.2006.03.048.
Sobel, E.R., Oskin, M., Burbank, D., Mikolaichuk, A., 2006b. Exhumation of basement-cored uplifts: example of the Kyrgyz Range quantified with apatite fission track thermochronolgy. Tectonics 25. https://doi.org/10.1029/2005TC001809.
Sobel, E.R., Strecker, M.R., 2003. Uplift, exhumation and precipitation: tectonic and climatic control of Late Cenozoic landscape evolution in the northern Sierras Pampeanas, Argentina. Basin Res. 15, 431–451. https://doi.org/10.1046/j.1365-2117.2003.00214.x.
Spikings, R., Cochrane, R., Villagomez, D., Lelij, R. Van Der, Vallejo, C., Winkler, W., Beate, B., 2014. The geological history of northwestern south America : from pangaea to the early collision of the caribbean large igneous province (290 – 75 Ma). Gondwana Res. 41 https://doi.org/10.1016/j.gr.2014.06.004.
Spikings, R., Cochrane, R., Villagomez, D., Lelij, R. Van Der, Vallejo, C., Winkler, W., Beate, B., der Lelij, R., Vallejo, C., Winkler, W., Beate, B., Lelij, R. Van Der, Vallejo, C., Winkler, W., Beate, B., 2015. The geological history of northwestern south America: from pangaea to the early collision of the caribbean large igneous province (290–75Ma). Gondwana Res. 27, 95–139. https://doi.org/10.1016/j.gr.2014.06.004.
Spikings, R., Seward, D., Winkler, W., Ruiz, G., 2000. Low temperature thermochronology of the northern Cordillera Real, Ecuador: tectonic insights from zircon and apatite fission track analysis. Tectonics 19, 649–668.
Spikings, R.A., Winkler, W., Hughes, R.A., Handler, R., 2005. Thermochronology of allochthonous terranes in Ecuador: unravelling the accretionary and post-accretionary history of the Northern Andes. Tectonophysics 399, 195–220. https://doi.org/10.1016/j.tecto.2004.12.023.
Tagami, T., Galbraith, R.F., Yamada, R., Laslett, G.M., 1998. Revised annealing kinetics of fission tracks in zircon and geological implications. Adv. Fission-Track Geochronol. 99–112. https://doi.org/10.1007/978-94-015-9133-1_8.
Vallejo, C., Spikings, R., Winkler, W., Luxieux, L., Chew, D., 2006. The early interaction between the Caribbean Plateau and the NW South American plate. Terra. Nova 18, 264–269.
Van der Hammen, T., 1960. Estratigrafía del Terciario y Maestrichtiano continentales y tectogénesis de los Andes Colombianos, Informe No. 1279. Serv. Geológico Nac. Bogotá 1961, 181–188.
van der Lelij, R., Spikings, R., Mora, A., 2016. Thermochronology and tectonics of the mérida Andes and the santander massif, NW south America. Lithos 248, 220–239.
Vermeesch, P., 2009. RadialPlotter: a Java application for fission track, luminescence and other radial plots. Radiat. Meas. 44, 409–410.
Villagómez, D., Spikings, R., 2013. Thermochronology and tectonics of the central and western cordilleras of Colombia: early cretaceous–tertiary evolution of the northern Andes. Lithos 160–161, 228–249. https://doi.org/10.1016/j.lithos.2012.12.008.
Villagómez, D., Spikings, R., Magna, T., Kammer, A., Winkler, W., Beltrán, A., 2011a. Geochronology, geochemistry and tectonic evolution of the Western and Central cordilleras of Colombia. Lithos 125, 875–896. https://doi.org/10.1016/j.lithos.2011.05.003.
Villagómez, D., Spikings, R., Mora, A., Guzmán, G., Ojeda, G., Cortés, E., Van Der Lelij, R., 2011b. Vertical tectonics at a continental crust-oceanic plateau plate boundary zone: fission track thermochronology of the Sierra Nevada de Santa Marta, Colombia. Tectonics 30. https://doi.org/10.1029/2010TC002835.
Vinasco, C., Cordani, U., 2012. Reactivation episodes of the Romeral Fault system in the northwestern part of central Andes , Colombia , through 39 Ar- 40 Ar and K-Ar results. Boletín Ciencias la Tierra 32, 111–124.
Vinasco, C., Cordani, U.G., González, H., Weber, M., Pelaez, C., 2006. Geochronological, isotopic, and geochemical data from Permo-Triassic granitic gneisses and granitoids of the Colombian Central Andes. J. South Am. Earth Sci. 21, 355–371.
Yamada, R., Murakami, M., Tagami, T., 2007. Statistical modelling of annealing kinetics of fission tracks in zircon; Reassessment of laboratory experiments. Chem. Geol. 236, 75–91. https://doi.org/10.1016/j.chemgeo.2006.09.002.
Zapata, J., Cardona, A., Restrepo, J.J., Martens, U., 2017. Geoquimica y geocronología de las rocas volcanicas basicas y el Gabro de Altamira, Cordillera Occidental (Colombia): registro de ambientes de plateau y arco oceanico superpuestos durante el Cretácico. Boletín Geol. UIS 39, 13–30.
Zapata, S., Cardona, A., Jaramillo, J.S., Patiño, A., Valencia, V., León, S., Mejía, D., Pardo-Trujillo, A., Castañeda, J.p.P., 2019a. Cretaceous extensional and compressional tectonics in the Northwestern Andes, prior to the collision with the Caribbean oceanic plateau. Gondwana Res. 66, 207–226. https://doi.org/10.1016/j.gr.2018.10.008.
Zapata, S., Cardona, A., Montes, C., Valencia, V., Vervoort, J., Reiners, P., 2014. Provenance of the Eocene soebi blanco formation, bonaire, leeward antilles: correlations with post-eocene tectonic evolution of northern south America. J. South Am. Earth Sci. 52, 179–193. https://doi.org/10.1016/j.jsames.2014.02.009.
Zapata, S., Sobel, E.R., Del Papa, C., Glodny, J., 2020. Upper plate controls on the formation of broken foreland basins in the Andean retro-arc between 26 and 28° S: from Cretaceous rifting to Paleogene and Miocene broken foreland basins. G-cubed, e2019GC008876.
Zapata, S., Sobel, E.R., del Papa, C., Muruaga, C., Zhou, R., 2019b. Miocene fragmentation of the Central Andean foreland basins between 26 and 28°S. J. South Am. Earth Sci. 94, 102238. https://doi.org/10.1016/j.jsames.2019.102238.
Zaun, P., Wagner, G.A., 1985. The potential of zircon fission track studies for deep-drilling projects. Naturwissenschaften 72, 143–144.